Measurements of the energy distribution of W atoms sputtered by low energy Ar ions using high-resolution Doppler spectroscopy

S. Ertmer, O. Marchuk, S. Dickheuer, S. Brezinsek, P. Börner, J. Schmitz and A. Kreter.

Forschungszentrum Jülich GmbH - Institut für Energie- und Klimaforschung - Plasmaphysik, Partner of the Trilateral Euregio Cluster (TEC), 52425 Jülich, Germany

E-mail: s.ertmer@fz-juelich.de

are in excellent agreement with the literature data.

Abstract. Emission spectra of neural tungsten (W) sputtered by impact of argon (Ar) ions in a weakly magnetized (≤ 0.1 T) Ar plasma were measured using a high resolution spectrometer at normal incidence angle to the surface. The measurements were performed for the mono-energetic impact energies between 70 and 150 eV using the neutral tungsten (W I) line at 4982.593 Å. The line shape of this line was simulated using a Doppler-shifted emission model to determine the energy distribution. Additional broadening mechanisms were taken into account: instrumental broadening, Zeeman effect and finally the photon or light reflectance at the W surface. The obtained energy distribution was found in a very good agreement with the Thompson distribution, even though deviations for lower impact energies are observed, e.g., the high-energy tail of sputtered particles demonstrates a faster drop compared to $1/E^2$ at energies below 100 eV. Moreover, the standard cosine (Knudsen law) distribution provides a rather good description of emission spectra in the energy range of study. Finally, the energy distribution was also compared with simulations carried out with the binary collision approximation (BCA) based Monte-Carlo code SDTrimSP. It shows a marginally worse description at low energies and

better description of the high energy tail compared to the Thompson one. Furthermore, the model was used to determine *in-situ* the degree of light reflection at the W surface. The results

1. Introduction

Sputtering occurs in various plasma applications, e.g. in magnetrons, hollow cathode lamps or fusion devices: energetic particles strike the plasma facing components and release neutral atoms. In many cases it is important to know the energy distribution of the sputtered particles. For instance in fusion devices, where the main source of sputtered atoms is the divertor, the energy distribution remains the critical issue for assessment of its lifetime. On the other hand, the parameters of energy distribution are also extensively used as the input in plasma codes. Because of many beneficial properties, like low erosion rates and its high melting point, tungsten seems to be the most promising material for the divertor [1]. The penetration depth of sputtered W atoms into the plasma depends on the energy of the sputtered atoms. Thus, without knowledge of the energy distribution of the sputtered atoms, it is hardly possible to determine the local cooling of the plasma, which is caused for example by line radiation [2].

The major sputtering mechanism of W atoms are collisions with high Z impurity ions. Until

now, however, the measurements of energy and angular distribution in energy range relevant in fusion for W at a few tens eV and below as in case of detachment are extremely limited. So for instance, the most accurate measurements for W sputtered by Ar were performed by Goehlich using the laser induced fluorescence from 5 keV down to 300 eV at normal incidence [3]. The stronger fall-off of the high energy tail compared to the Thomson-Sigmund [4] distribution was observed for the energies below 1 keV. A very good agreement was obtained with TRIM.SP [5] code. By looking at the angular distribution the situation is rather unclear. So, for instance, the theoretical expectation for W sputtered by Ar ions at 100 eV demonstrates cosine distribution [6]. On the other hand the measurements in the plasma using rotating target and mass ion spectrometer demonstrated a heart shaped profile [7].

In this paper we investigate energy distribution of W atoms sputtered by Ar ions with monoenergetic impact energies between 70 and 150 eV, relevant for plasma wall interaction in fusion devices. For this purpose we used the emission spectra measured in the low-density plasma of the linear plasma device PSI-2 with a high-resolution spectrometer. The fact that spectroscopy could determine the energy distribution of sputtered atoms was recalled in a recent theoretical work [8]. With this paper we fill this gap. Second, the operation range of PSI-2 plasma with electron density of 10^{10} - 10^{12} cm⁻³ excludes the collisional line broadening mechanism in front of the target. In this case neither the ion nor the electron temperature plays the role for the line shape (the main source of excitation of the sputtered atoms remains electron impact excitation). Finally, the high resolution emission spectroscopy was successfully applied to the problem of emission of reflected atoms demonstrating the effects of light or photon reflection on line shapes [9].

2. Instrumental setup

In this experiment a mirror-like polished quadratic tungsten sample $(1.3 \, \mathrm{cm} \times 1.3 \, \mathrm{cm})$ was exposed to an Ar plasma in the linear plasma device PSI-2, which is described in detail elsewhere [10]. The diameter of the hollow profiled cylindrical plasma column was in the order of 10 cm. The sample was positioned in the electron density $(n_e \approx 2 \times 10^{12} \, \mathrm{cm}^{-3})$ and temperature $(T_e = 3 \,\mathrm{eV})$ maximum. By applying the negative potential to the target the plasma ions were accelerated onto the sample to mono-energetic energies between 70 and 150 eV. The sample temperature was kept at about 300 K due to water cooling. A high resolution spectrometer $(\frac{\lambda}{d\lambda} \approx 7 \cdot 10^5)$ with an Echelle grating in the Littrow configuration was used to observe the line radiation of the sputtered tungsten atoms in front of the target. For this purpose, the lineof-sight was adjusted parallel to the magnetic field lines and parallel to the target normal (the observation angle $\theta=0^{\circ}$). The line-of-sight was focused trough the PSI-2 cathode onto the target surface in about 2 m distance. Back side illumination resulted in a spot size of approximately 0.3-0.4 cm on the target. The light emission of the sputtered atoms occurs dominantly in the first cm in front of the target [12]. The mean free path $\lambda_{\rm mfp}$ for the sputtered atoms before colliding with the Ar⁺ ions was in the order of 10 m. As a consequence, collisions of the sputtered atoms with the ions can be neglected. Since the ionization degree of the PSI-2 plasma is only a few percent, collisions with the background gas are more probable. Nevertheless, these can also be neglected, since the the mean free path, in this case, was still in the order of a few 10 cm. This means, the sputtered atoms moved in a first order freely and without collisions with atoms or ions in the observation volume. As the ionization length for the sputtered atoms $\lambda_{\rm ion}$ was in the order of 20 cm, most atoms leave the observation volume due to geometric effects corresponding to the angular distribution of the sputtered atoms and not by ionization. However, in contrast to fusion plasma, where the transition with 4008.751 Å is routinely measured the line at 4982.593 Å was selected instead [11]. There are a few reasons for this. Firstly, the line 4008.751 Å originates from metastable level with the energy of about 0.37 eV above the ground one. It is not resolved until now if this level populated during sputtering or by the collisional or radiative distribution

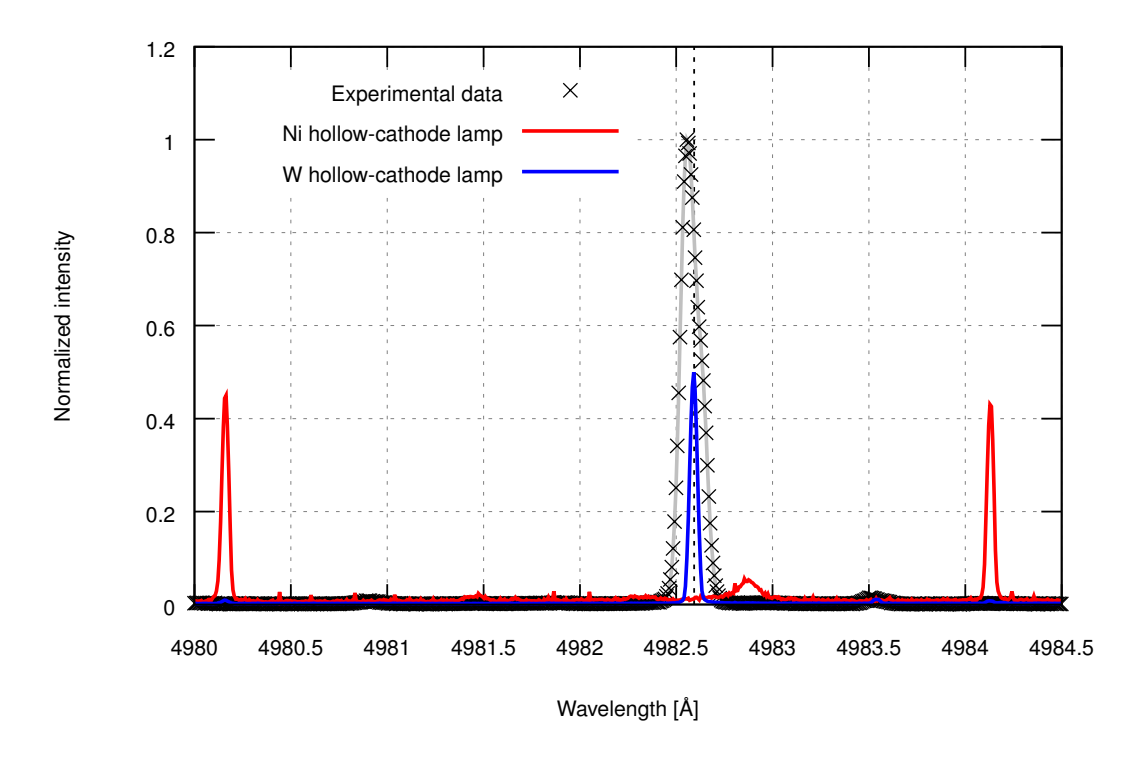


Figure 1. Example of the spectra measured by the high resolution spectrometer. The spectrum from Ni hollow cathode lamp was used for calculating the dispersion (red line). The spectrum from W I line was used to determine the unshifted wavelength of observed transition and instrumental FWHM (blue line). The spectrum of the exposed W target, where the Ar ions had the impact energy of 150 eV, is shown by the black crosses.

(cascades) in the plasma itself [12]. Secondly, the $\Delta J=1$ transition, where J is the total angular momentum, at 4982.593 Å originates from the ground level with J=0. Therefore, the Zeeman pattern remains extremely simple as only two σ lines, corresponding to transition with $\Delta M=\pm 1$, and one π component with $\Delta M=0$ are emitted. Here, M is the magnetic quantum number. At the line-of-sight being parallel to the magnetic field only the two σ lines with $\Delta M=\pm 1$ can be detected. Finally, this transition is by no means weaker in comparison with 4008.751 Å. Nevertheless, this transition at 4982.593 Å was already studied in [14], where a discrepancy in between the experimental data and ADAS database [15] calculations was found. Thus, further investigation of this transition is necessary. The experimental data analyzed in this work was also shown in [16].

The spectrometer was calibrated by fitting the line radiation of the Ni and W hollow cathode lamps. The Ni I lines at 4980.16 Å [11] and 4984.13 Å [11] were fitted with a Voigt profile to determine the dispersion of the spectrometer before the measurements. The W I line was used to determine the instrumental full width half maximum (FWHM = 5 channels) of the same W I line as used in experiments. The calibration spectrum of the Ni lamp is shown in the Figure 1 (red curve) in combination with an experimentally measured spectrum (black crosses and gray line) of sputtered W in PSI-2 and W I lines from the hollow cathode lamp (blue curve). As one can immediately see the instrumental broadening constitutes about 15-20% of the measured line width in the plasma so that this fact must be taken into account.

3. Modeling of emission spectra

The modeling of emission spectra consists of two parts. Firstly, the spectroscopic part, which uses as input a parameterized energy distribution function. In the second part this spectrum is modified by fitting the synthetic to the spectrum measured at PSI-2, so that finally the new distribution function, which provides the best description of the experimental spectrum, is achieved. Thus the approach itself does not differ from the standard technique for derivation of plasma parameters such as electron density or temperature.

Without doubt for high impact energies of a few hundred and above electron volt of the incoming particles (ions) the Thompson energy distribution [17] was shown to be the most successful one [18]. For this reason the energy distribution function using the Thompson formula was selected as initial one:

$$\Phi(E,\theta) = G(\theta)F(E) \tag{1}$$

$$G(\theta) = \frac{1+b}{2\pi} \cos^b(\theta) \tag{2}$$

$$F(E) = C \frac{E(1 - \sqrt{E/E_m})}{(E + E_b)^{n+1}}$$
(3)

Here, $\Phi(E,\theta)$ is the resulting function, E is the energy of the sputtered particles outside the solid, E_b is the surface binding energy, which was set to 8.7 eV [19], E_m is the maximum recoil energy of the atoms and C is the normalization constant at the condition $\int_0^{E_m} F(E) dE = 1$. The parameter n=2 corresponds to the Thompson distribution and the parameter b=1 corresponds to a cosine angular distribution. By matching the experimental spectrum with the spectroscopic model we derive the new value of n and the parameter b. Whereas n is responsible for the high energy-tail of the energy distribution and b defines if the angular distribution is under-cosine (b < 1), cosine (b = 1) or over-cosine (b > 1). One should also admit that in general, the separation of the energy distribution into the angular and energy factors is not always possible. However, for the ions at normal incidence as in the plasma sheath, one expects a relatively low modification [6].

In addition to the Thompson distribution we also used Monte-Carlo SDTrimSP [20] calculations for further comparison with experimental data.

In Figure 2 the calculated energy distribution of W atoms sputtered by Ar ions with an impact energy of 150 eV is shown. The distribution results from calculations with the recent SDTrimSP version 6.01, where the interaction of 10⁸ Ar⁺ ions with a W solid was modeled. For the calculations, the surface binding energy model isbv=1 with $E_{\rm b}(W)=8.79$ was chosen and for the interaction potential the "krypton-carbon potential" was used. The SDTrimSP data is displayed in the figure by a step function in blue as it represents a histogram of the output data of the Monte-Carlo simulation. The continuous curve is the result of the fit of the SDTrimSP data using equation (3) being further used by the spectroscopic model. The standard Thompson distribution is shown by the green curve. In general the agreement between the Thompson and SDTrimSP calculations is in low energy range is satisfactory. So, for instance, in the region of 5-20 eV one detects only a shift by a few eV between two profiles. The Thompson energy distribution shows a stronger increase for the first few eV, whereas the SDTrimSP data suggests a later maximum but a stronger decrease of the distribution for higher energies. In [5] it is reported, that BCA based codes, like SDTrimSP, become inaccurate for low impact energies, since many-body effects become relevant. As the Doppler-shifted emission model used in this work is in need of an parameterized energy distribution for input parameter and is based on the Thompson energy distribution given by equation (3), the energy distribution simulated by SDTrimSP was fitted by this equation. This resulted in the following parameter values: $E_b = 23 \,\mathrm{eV}, n = 3.8$ and the maximal recoil energy $E_{\rm max}$ was reduced from 88 eV to 53 eV. It needs to be noted, that

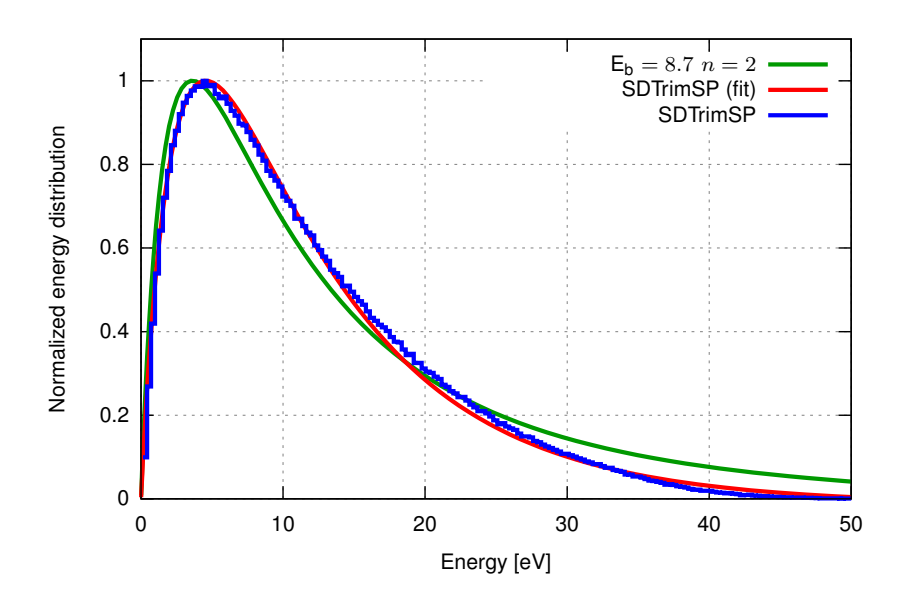


Figure 2. Energy distribution function of W atoms at Ar⁺ ions impact of 150 eV from SDTrimSP and Thompson. The SDTrimSP data is shown using blue color. The fit with equation (3) of the SDTrimSP energy distribution is displayed in red. The Thompson distribution is shown in green.

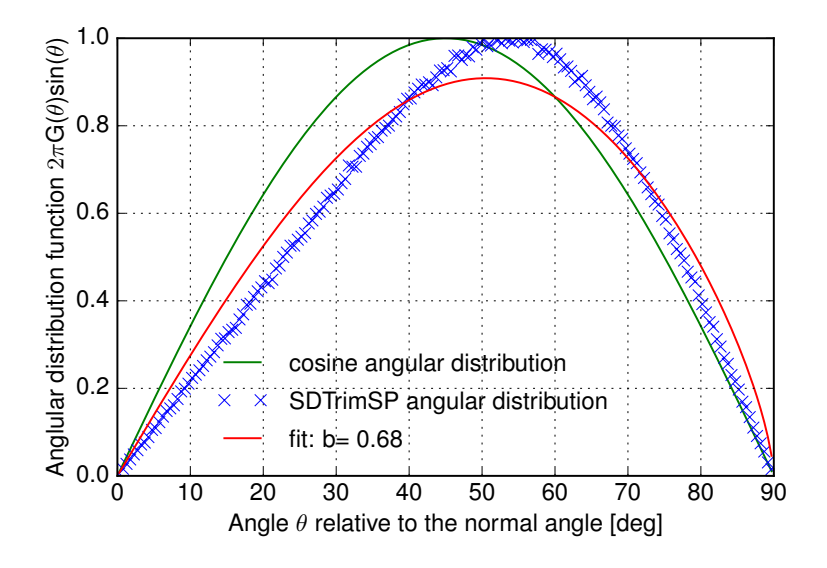


Figure 3. Angular distribution function of W atoms at Ar ions impact of 150 eV calculated by SDTrimSP. The SDTrimSP data are shown using blue color. The fit with the equation (3) is displayed in red. The cosine distribution is shown in green.

the combination of E_b and n in equation (3) defines the position of the most probable energy of the sputtered atoms. An increase in E_b leads to a shift of this position to higher energies. In contrast an increase in the parameter n leads to a shift of this position to lower energies and furthermore to leads to a stronger fall-off of the high energy tail of the energy distribution function. Thus, E_b is a fitting parameter in this work, whereas in the original work [17] where n equals 2, this represents the physical surface binding energy. However, similar observations

of an increased E_b in combination with increased parameter n were detected also by Goehlich [3]. In [3] the best agreement of experimental data with the Sigmund-Thompson distribution for impact energies of 300 eV was found for an slightly increased E_b of $\approx 10 \,\text{eV}$ and an increased parameter n. This slightly increased binding energy is in good agreement with simulations of the sputter yield based on the binary collision approximation in [13].

The similar procedure was applied for the angular distribution. For parameter b the value of 0.68 (the Figure 3) provides a reasonable description of SDTrimSP data, instead of b=1 corresponding to the cosine (Kundsen law) distribution.

The spectroscopic model for Doppler-shifted emission we use, was first applied in [16] on spectra of sputtered aluminum atoms and originates from the model used for study backscattered (reflected) hydrogen atoms [21]. In both cases the model assumes a point source as origin for the emitting atoms, which is a good approximation for an observation parallel to the target normal. The spot size of the line of sight on the target surface has a diameter of approximately 3 mm and the size of the quadratic target is 13 mm. As reported in [12], the emission of the observed transition occurs nearly only in the first centimeter in front of the target. Therefore, the characteristic length of emission is lager than the spots size and most atoms sputtered inside the spot of the line of sight emit only inside the observed emission volume. Only atoms at small grazing angle leave the observed emission volume and emit also outside of this volume. However, the emission of this particles is replaced by emission of particles sputtered outside the spot. Assuming an atom A is sputtered inside the observation spot and an atom B is sputtered in a distance of diameter of the spot. If atom A leaves the observation volume, atom B enters at the same angle and energy, since both atoms are sputtered at same experimental conditions, as density profile is broader than the target size. Thus, the assumption of a point source is valid and the distribution functions can be modeled precisely. However, the point source approximation has its limit. For instance, in the extreme case of an observation angle parallel to the surface, the point source is transformed to a line. Equidistant lines and not points contribute to the emission spectrum and the point source assumption is not valid, so that 2D extension of source of the Doppler-shifted model is required. Therefore, so far, only the observation parallel to the surface normal can be modeled accurate. This means only each one distribution functions can be determined by this model, since one emission spectrum can be modeled with different combinations of energy and angular distributions.

The major difference between experimental results of sputtered and backscattered atoms, except for the fact that the energy distribution function as well as the source of excitation are completely different, represents the significant instrumental broadening in the spectrum of the sputtered atoms compared to the spectrum of the backscattered atoms. In the new case the observed signal represents the convolution of the spectral radiance and the instrumental broadening. Therefore, for the arbitrary observation angle θ_0 relative to the surface normal, the observed intensity i on the detector at the wavelength λ_i is described by the following expression:

$$i(\lambda_i, \theta_0) = \int_{-\infty}^{\infty} L(\lambda, \theta_0) V(|\lambda - \lambda_i|, \delta_L, \delta_G) d\lambda.$$
 (4)

Here, L is the spectral radiance at the wavelength λ and $V(|\lambda - \lambda_i|, \delta_L, \delta_G)$ is the instrumental function. We selected the latter one using the Voigt profile, where δ_L and δ_G are the Lorentzian and Gauss widths obtained from the spectra of the Ni and W cathode lamps. The observed spectral radiance consists of two parts. The first one or the blue-shifted part is the result of the direct emission and the second (red-shifted) part is the result of photon or the light reflection at the surface [21]. The surface operates as mirror, irrespective on the question if the emission in front of it is caused by backscattered or sputtered atoms. The effect of light reflectance at the target surface onto the emission spectrum of sputtered atoms, especially on the red-shifted component, was studied in reference [16] for aluminum. A reduction of the degree of reflectance

at the target surface leads to a reduction of the intensity of the red-shifted component in relation to the blue-shifted component. Different angular distributions for the red shifted and the blue shifted component are not considered in the model yet. this becomes necessary for light diffusive targets, where the angular distribution of the red shifted reflected component has to be cosine. The observed spectral radiance is non-zero for all the wavelengths λ with $\Delta \lambda_p = \lambda - \lambda_p$ and $|\Delta \lambda_p| \leq |\Delta \lambda_m|$. λ_p is the wavelength of the Zeeman multiplet with the unshifted wavelength λ^0 and $\Delta \lambda_m$ corresponds to the Doppler shift with the maximal energy E_m of sputtered atoms:

$$L(\lambda, \theta_0) = 1/(4\pi)N_{\rm w}n_e \sum_p r_p(\theta_0)A_p \left(\epsilon(\Delta\lambda_p, \theta_0) + R(\lambda^0)\epsilon(-\Delta\lambda_p, \theta_0)\right), \tag{5}$$

with $r_p(\theta_0)$ being the angular factor corresponding to the linear or to the circular polarizations of the component p, $R(\lambda^0)$ is the optical reflectance of the surface at λ^0 and $N_{\rm w}$ is the density of the tungsten atoms. For transition with $\Delta M=\pm 1$ the angular factor $r_p(\theta_0)=(1+\cos^2(\theta_0))/2$ and for $\Delta M=0$ the factor $r_p(\theta_0)=\sin^2(\theta_0)$. The parameter A_p is the relative theoretical intensity of Zeeman component and $\epsilon(\Delta\lambda_p,\theta_0)$ is the emission rate coefficient. The sum over p extends over all components of the Zeeman multiplet.

Indeed, the experiments are performed in a weakly magnetized plasmas of up to $100 \,\mathrm{mT}$. At the assumption that the Landé factor $g_j = 1$, we estimate the strength of the magnetic field, which produces a splitting of the spectral lines equal to the Doppler shift for atoms leaving the surface with their binding energy, by the expression:

$$B[T] \approx \frac{1}{\lambda_0[\mu m]} \sqrt{\frac{E_b[eV]}{M[u]}}.$$
 (6)

Here M is the mass of the sputtered atoms in atomic mass units, λ_0 is the observed wavelength in μm , E_b is the surface binding energy in eV and B is the magnetic field in T. Thus for the characteristic surface binding energy $E_b = 10\,\mathrm{eV}$, the mass of sputtered atoms M=184 u and wavelength λ_0 of 0.5 μ m the magnetic field of approximately 450 mT causes the splitting comparable with the energy of the atoms of 10 eV. Considering that in the case of Thompson distribution the maximum the energy distribution function is at the energy of $E_b/2$ only the magnetic field of 10-20 mT represent the critical field beyond which the Zeeman effect must be included. Thus in contrast to the emission spectra of backscattered atoms, the Zeeman effect has to be taken into account for studies of emission spectra of sputtered atoms. In the limit of a high magnetic field the Zeeman effect could be used to determine the magnetic field. In [22] the magnetic field of the Tokamak TEXTOR was modeled from the line shape of sputtered tungsten. However, it was not possible in to determine the energy or angular distribution of the sputtered atoms.

Finally, for the W I transition selected in this work all intensities A_p are equal, i.e. the assumption on the statistical population of excited magnetic levels is not necessary for this line. In the model the temporal evolution of the electron density, and thus the influence of the Langmuir-Debye-sheath in front of the target on the excitation, is neglected. This assumption is valid, since the maximum of emission is located in the order of 2 mm in front of the target [12], whereas the sheath of a biased target is in the order of a few times the Debye length [23], which is in our experimental conditions a few times $\approx 1 \times 10^{-2}$ mm. Therefore, the emission rate coefficient $\epsilon(\Delta \lambda_p, \theta)$ is expressed using the same formula as in [21]:

$$\epsilon(\Delta \lambda_p, \theta) = \int_{v} \langle \sigma v \rangle f(\mathbf{v}) dv^3, \tag{7}$$

where $\langle \sigma v \rangle$ is the temporal constant excitation rate coefficient of sputtered atoms by an electron impact and $f(\mathbf{v})$ is the velocity distribution function of sputtered atoms in the velocity

space:

$$f(\mathbf{v})dv^3 = \Phi(E,\theta)d\Omega dE,\tag{8}$$

with the solid angle $\Omega = 2\pi \sin(\theta)d\theta$ and the kinetic energy $E = Mv^2/2$. The integral of the velocity distribution defined as: $\int f(\mathbf{v})dv^3 = 1$. Finally, the Doppler-shift is taken into account via:

$$\Delta \lambda_p / \lambda_p = \mathbf{v} \mathbf{e}_{\theta_0} / c. \tag{9}$$

Here, c is the speed of light and \mathbf{e}_{θ_0} is the unity vector along the line-of-sight. The line intensity or the net emission equals to:

$$I_0 = \int_{-\infty}^{\infty} i(\lambda, \theta_0) d\lambda. \tag{10}$$

It remains independent on the observation angle. The integration in equation (7) was performed by matching the coordinates of the velocity vector of the sputtered atoms emitting in the hemisphere to the cylindrical coordinate system, rotating on the angle θ_0 defined by the line-of-sight.

4. Experimental Results

The experimental spectra is shown in the Figure 1. For modeling the following parameters were varied: the normalization constant between the experimental spectra and the theoretical one, the value of spectral reflectance and one of the parameter of the Thompson distribution, e.g. the parameter b or n. The only parameter that we had to take from other measurements was the value of magnetic field (B=85 mT) being indispensable for correct description of the spectra. This value relies on extrapolation of the TDLAS (Tunable Diode Laser Absorption Spectroscopy) measurements on metastable Ar recently presented in [24]. The example of the modeling is exemplified in the Figure 4. For all modeled spectra a cosine angular distribution (b=1) based on the results in [6] was chosen. The upper part of the figure displays single elements of the Doppler-shifted emission model. In green the spectrum only resulting from cosine angular distribution and standard Thompson energy distribution (n=2, $E_b=8.7\,\mathrm{eV}$ and $E_{\mathrm{max}}=88\,\mathrm{eV}$) is shown. In gray the measured spectrum of the W hollow cathode lamp is shown. This spectrum was used to determine the instrumental broadening. The black bars in the figure show the position of the σ components calculated for a magnetic field of 85 mT. The lower part of the figure displays the spectra modeled taking all elements shown in the upper part into account. The agreement between the measured and modeled spectrum is rather good for the green line. This spectrum results from fitting the modeled spectrum to the measured spectrum via variation of the parameter n. The whole spectral range of emission, i.e. the blue and the red shifted part, is accurately described using this parameters, which are also matching the standard Thompson distribution. Only the high energy wings of emission show a slight deviation. They correspond to the wavelength lower than 4982.5 Å and larger than 4982.7 Å. The calculation with n=1(yellow curve) and n=3 (purple curve) are also shown for comparison. In case of n=3 neither the central part nor the wings of emission could be accurately described. The spectrum is too narrow. On the other hand, by selecting n=1 the line shape is too broad and also in this case the description of the measured spectrum is not possible. Thus, the original Thompson distribution provides a very accurate description of the spectrum without any modification. Our results at 150 eV are by no mean in contradiction with the LIF results of Goehlich [3]. In the description of the LIF data it is relied on the Thompson-Sigmund distribution [4] which in comparison to Thompson distribution [17] neglects the $1 - \sqrt{E/E_m}$ factor in expression (3). Whereas at the energies $E \leq E_b$ this factor is of no importance, this factor leads to a reduction of the high energy tail in the energy distribution function.

The experimental data and the best fit with n = 1.97, as shown in Figure 4 in green, are exemplified in Figure 5 in velocity and energy units. Here, instead of spectral radiance, the

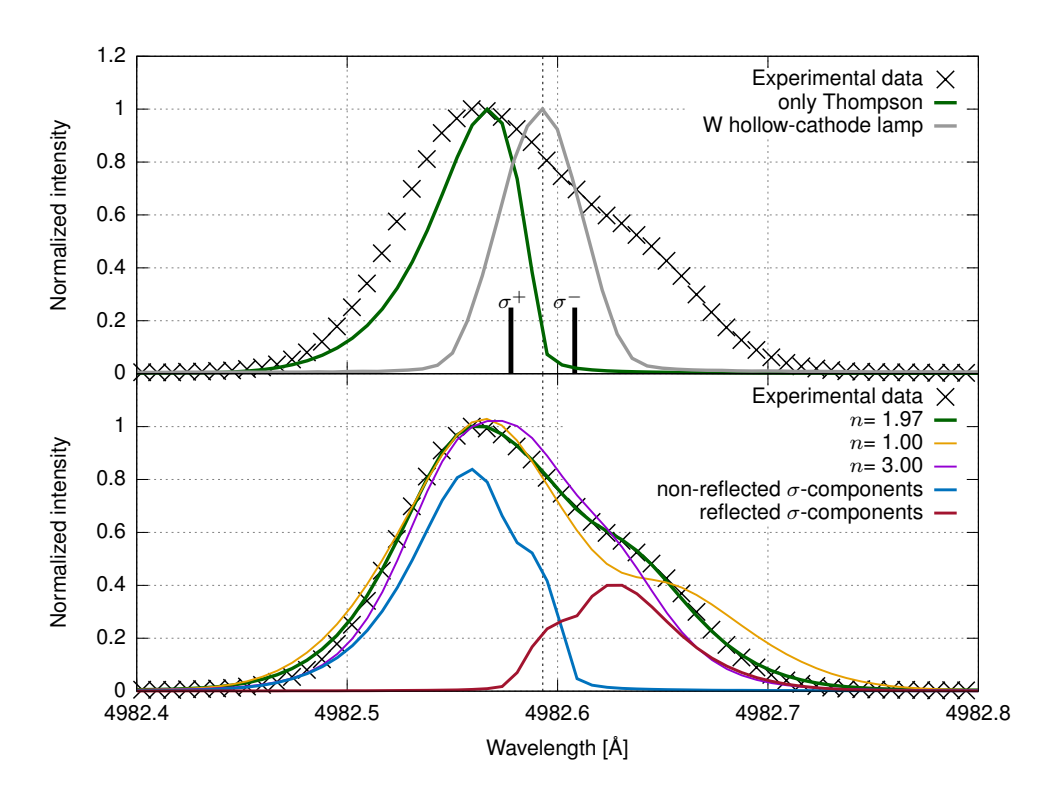


Figure 4. Modeling of the measured spectrum of sputtered tungsten in the Ar plasma with the impact energy of the incident ions of 150 eV. The Experimental data is given by the black crosses. The vertical black dashed line shows the position of the unshifted line. Here, for the modeled spectra the angular distribution was assumed to be cosine (i.e. b=1) [6] and the binding energy $E_b = 8.7 \,\mathrm{eV}$ [19]. In the upper part of the figure in green the spectrum resulting from the standard Thompson energy (i.e. n=2) is shown, without taking broadening and Zeeman effect into account. The black bars the splitting caused by magnetic field of 85 mT with a Landé factor $g_j = 1.54$ [11]. The spectrum of the hollow cathode lamp where the broadening for the model was taken from is shown in gray. In the lower part modeled spectra for different n taking all mentioned effects into account is shown. The best agreement is found for n = 1.97 (green). For smaller n values (yellow) the curve shows a stronger pronounced deformation vice versa for n higher than 2 (purple). The blue- and red- curves show the spectral radiance of the direct and reflected signals without taking the instrumental broadening into account on bases of the green curve.

modeled red- and blue-shifted signal, taking into account the instrumental profile according to equation (4), the Doppler-shift and the Zeeman splitting, is depicted. The x-axis displays the velocity component and the Doppler shift in energy units of the emitted light, normal to the target surface. At the observation angle of 0° only a positive velocity component for the non-reflected signal is possible, vice versa for the reflected signal. But due to the instrumental broadening and Zeeman splitting there is an overlap between modeled components. The modeling takes it into account and remains to be in an excellent agreement with experimental data up to the energies of $20\,\mathrm{eV}$. Above this energy the modeled fraction of sputtered atoms overestimates the experimental data. The ratio between the components delivers the optical property of the W surface, i.e. the light reflectance. The fit provides the ratio R = 0.55, which also in a very good agreement with literature values for W of 0.53 in [25].

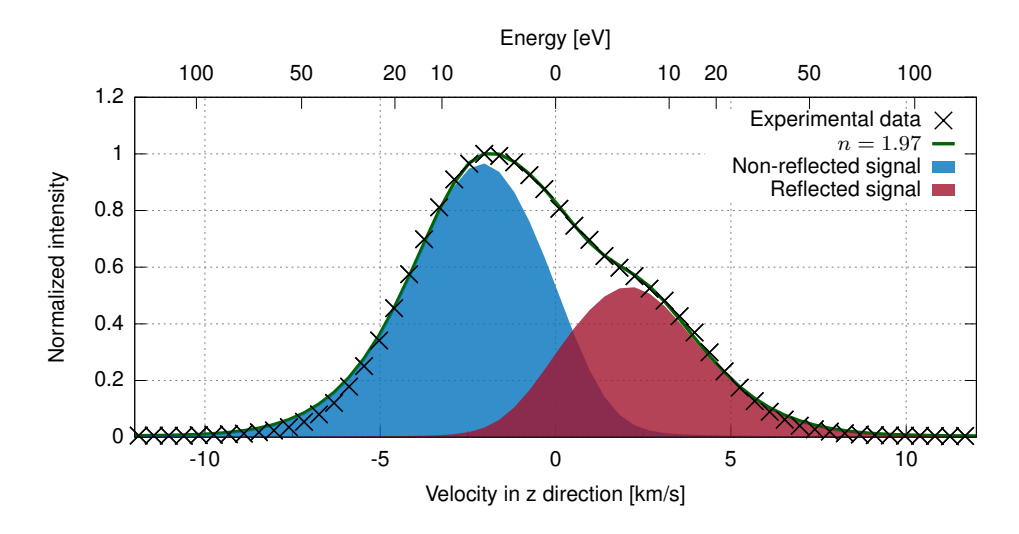


Figure 5. Shown is the emission spectrum at 150 eV for the Ar⁺ ions by black crosses, the best fit of the model in green and the reflected and the non-reflected component. The x-axis is the velocity component in the z direction, which is the observation direction, normal to the target surface. The velocity was also converted in energy shift, which is the second x-axis at the upper side of the Figure.

Additional to the impact energy of $150\,\mathrm{eV}$, we modeled the emission spectra of sputtered W atoms for different impact energies in the range of 70 to $130\,\mathrm{eV}$. The results are shown in the Figure 6 in velocity and energy units. The shape of the emission spectrum depends on the impact energy of the sputtering ions: for increasing impact energy the deformation of the line increases, the blue-shifted component moves more negative velocities, whereas the red-shifted component moves symmetrically to higher positive velocities. Under the assumption of a constant cosine angular distribution in this energy range the modeling of the emission spectra results in an increase of the fitting parameter n with decreasing impact energy of the sputtering ions. This tendency was observed practically in numerous experiments performed at higher energies [3, 18]. The parameter n varies from 2.2 at $70\,\mathrm{eV}$ to 1.97 at $150\,\mathrm{eV}$. Also the degree of light reflectance determined by the model is given for each case in the Figure 6. It is found to be in the range between 55% and 58%.

The comparison of the experimentally determined spectrum at 150 eV with different modeled spectra using SDTrimSP energy distribution is shown in the Figure 7. The spectrum resulting from the SDTrimSP energy and angular distribution (b=0.68) is shown in green. The description of the experimental data close to the unshifted wavelength and thus to lower energies is less accurate for all angular distributions compared to the Thompson distribution. This Figure reflects the behavior of the energy part shown in the Figure 2 as both distribution are quite close to each other at low energy below 20 eV. For the high energy tail the situation changes. The Thompson distribution overestimates the number of sputtered atoms, whereas in case of SDTrimSP the model reproduced also the energy tail quite well. Here we also exemplified the sensitivity of the model to the angular distribution. Fitting the angular distribution results in b=1.28 (red curve) and strong separation of the red and the blue shifted signal and therefore a too distinctive dent in the modeled spectrum in comparison to the experimental data. Finally, we also demonstrate an example with b=0.4 (purple curve) to exemplify the effect of the angular distribution onto the modeled spectrum. In this case the spectrum could be hardly described properly.

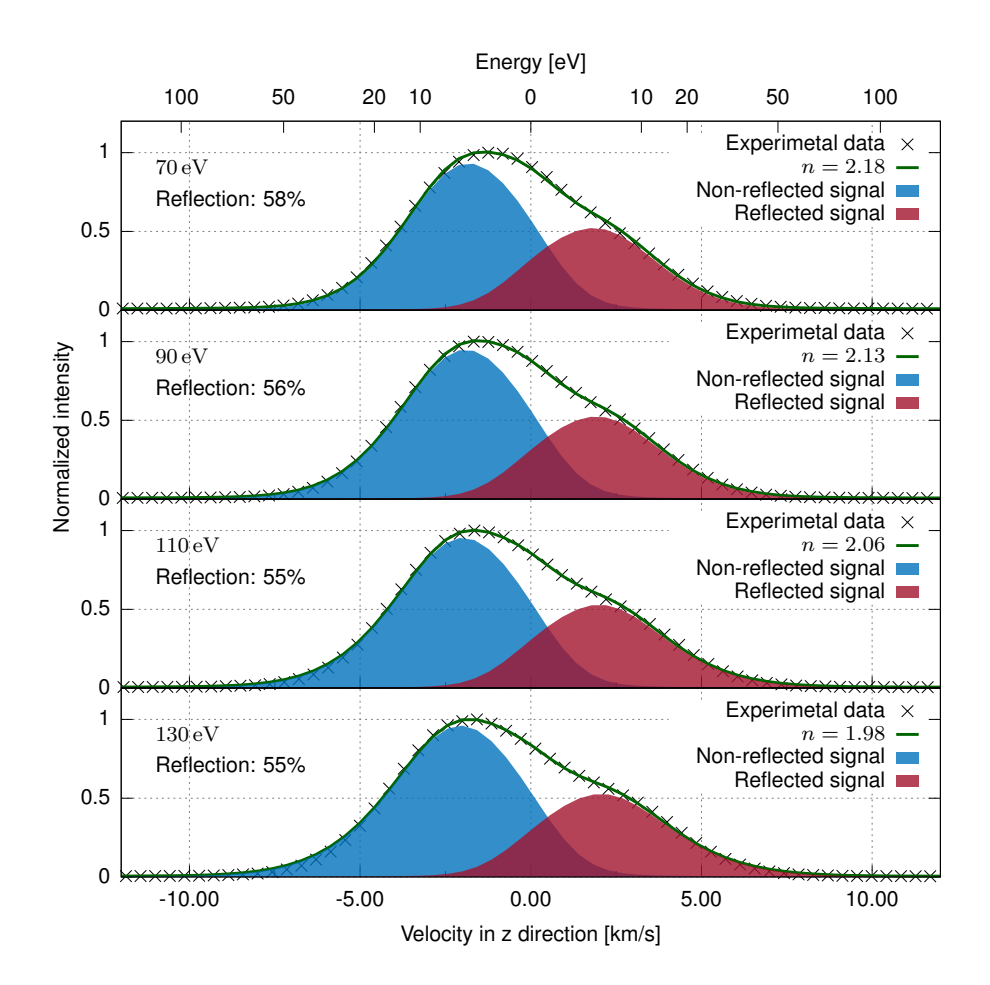


Figure 6. Shown is experimental data for different impact energies for the Ar ions in black and the modeled spectra in green. The fitting parameter n increases for decreasing impact energies. The degree of light reflectance was modeled and is displayed in the graph.

5. Discussion and conclusion

In this work, the energy distribution of sputtered tungsten for impact energies of $70\text{-}150\,\mathrm{eV}$ of Ar^+ ions at normal incidence was modeled from the emission spectra of the sputtered W atoms. For this purpose the measured line shape was fitted taking the Doppler-shift, Zeeman splitting, instrumental broadening and photon reflectance into consideration. The emission spectrum could be described using only three parameters: normalization constant, value of reflectance and parameter n of energy distribution function. Here, we selected the probably simplest line of W I emission as only two equal Zeeman components can be observed at the normal incidence. Nevertheless, the value of magnetic field had to be taken from elsewhere. It represents one of the uncertainties in the model.

In spite of the simplicity of the model, we obtain a quite accurate description of the spectra. The parameter n of the high energy tail in the expression of the distribution function deviates only by 10% from the Thompson one (n=2). It increases towards the energy of 70 eV to the value of 2.2. The surface binding energy equals to $8.7 \,\mathrm{eV}$.

Comparison with the SDTrimSP simulations demonstrates quite similar results. Whereas the description at the lower energies and thus at the unshifted wavelength is not as accurate as in

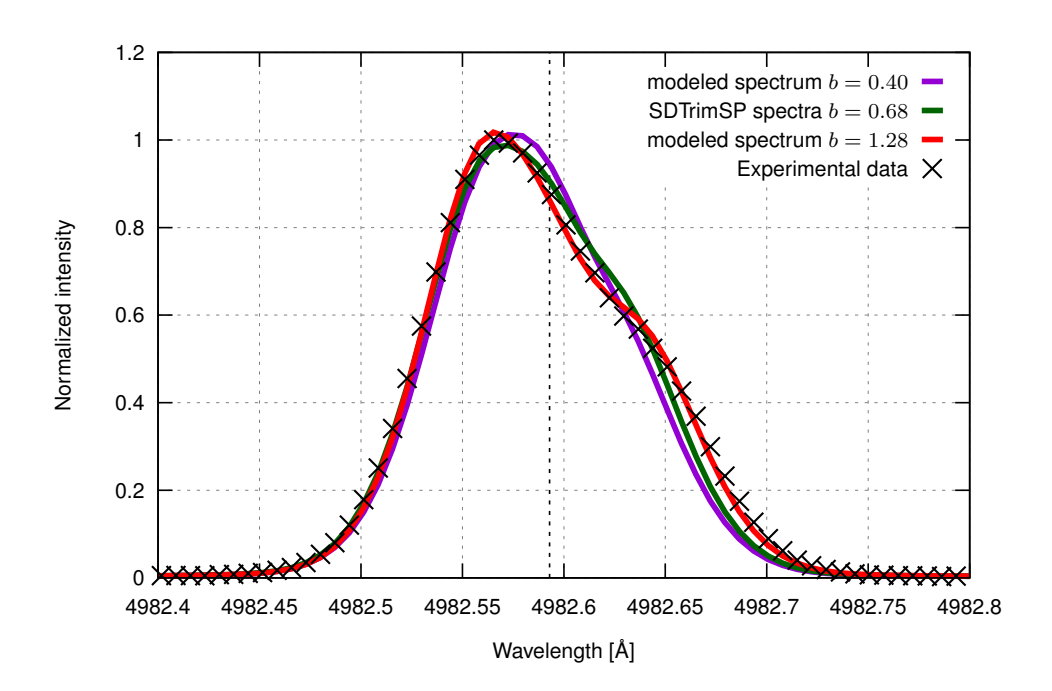


Figure 7. Comparison between the energy distribution modeled from the line shape at an impact energy of 150 eV in an Ar plasma (crosses) and SDTrimSP data (green) [5]. Furthermore, a fit with the equation (3) of the SDTrimSP energy distribution is displayed in red (b = 1.28). The simulation with b = 0.4 is shown using purple curve.

case of the Thompson one, the high energy tail shows a better description. The most surprising remains the situation with the angular distribution. In case of the Thompson distribution for the energy part we see no need in modification of the cosine angular distribution at all. Although, SDTrimSP simulations show the value of $b \approx 0.68$ at 150 eV impact energy, by fitting angular distribution via the Doppler-shifted emission model based on the SDTrimSP energy distribution to the experimental data results in a value of 1.28 for the parameter b. Selecting the strong under-cosine distribution function (b = 0.4), we could not really describe the spectrum well at any value of parameter n. Further reduction of sputtered atoms moving at normal incidence as in the case of heart-shaped distribution leads to very narrow emission. Our results confirm the theoretical expectations [6] but remains in clear contradiction to the experimental data [7]. One of the reason could be the surface morphology, e.g being already diffusive for particles, but remains the specular one for the visible wavelengths.

The forthcoming measurements of energy and angular distribution of sputtered atoms using Doppler-shifted emission can be further improved. On the one hand the measurements at other angles of observations seem to be straightforward providing additional reliability. Nevertheless, the interpretation of such data requires more extensive modeling as the point source approximation becomes invalid. On the other hand, one could potentially apply the high resolution spectropolarimetry to avoid the impact of magnetic field on the line shape of spectral lines at all. By the usage of a spectropolarimetry the single Zeeman-components could be optically isolated and therefore be observed independently. Thus, the impact of the magnetic field to the results of the modeling would be reduced. Furthermore, the magnetic field could be determined by this method. We are going to investigate this in the near future.

6. Acknowledgment

We thank Udo von Toussaint for valuable comments on the SDTrimSP code. This work has been carried out within the framework of the EUROfusion Consortium and has received funding from the Euratom research and training programme 2014-2018 and 2019-2020 under grant agreement No 633053. The views and opinions expressed herein do not necessarily reflect those of the European Commission.

7. References

- [1] B. Lipschultz et al., Nucl. Fusion 52, 123002 (2012), https://doi.org/10.1088/0029-5515/52/12/123002.
- [2] V. Philipps, J. Nucl. Mater. 415, (2011), https://doi.org/10.1016/j.jnucmat.2011.01.110.
- [3] A. Goehlich et al. J. Nucl. Mater. 266-269, (1999) 501-506, https://doi.org/10.1016/S0022-3115(98)00830-7.
- [4] P. Sigmund, Phys. Rev. 184 (1969) 383, https://doi.org/10.1103/PhysRev.184.383.
- [5] W. Eckstein "Computer Simulation of Ion-Solid Interactions", Springer-Verlag (1991).
- $[6] \ \text{M. Stepanova et al. } \textit{J. of Vacuum Science & Technology A } \textbf{19}, (2001) \ 2805, \\ \text{https://doi.org/} 10.1116/1.1405515.$
- [7] D. Nishijima et al. J. Nucl. Mater 415, (2011) 96-99, https://doi.org/10.1016/j.jnucmat.2010.12.017.
- [8] A. Sepetys et al. Plasma Phys. Control. Fusion 61, (2019) 125017, https://doi.org/10.1088/1361-6587/ab4f99
- O. Marchuk et al, J. Phys. B: At. Mol. Opt. Phys. 51, (2018) 025702, https://doi.org/10.1088/1361-6455/aa987d
- [10] A. Kreter et al. Fusion Science and Technology 68, (2015) 8-14, https://doi.org/10.13182/FST14-906.
- [11] A. Kramida, et al (2018) NIST Atomic Spectra Database (ver. 5.6.1) [Online] [2020, March 10].
- [12] S. Ertmer et al. conference proceeding 45th EPS Conference on Plasma Physics, (2018).
- [13] X. Yang et al. Appl. Surf. Sci. 293, (2014) 187-190, https://doi.org/10.1016/j.apsusc.2013.12.129
- [14] S. Brezinsek et al. Phys. Scr. T170, (2017) 014052, https://doi.org/10.1088/1402-4896/aa8a45
- [15] H. P. Summers (2004) "The ADAS User Manual, version 2.6" http://www.adas.ac.uk
- [16] S. Ertmer et al. Phys. Scr. T171, (2020) 01403, https://doi.org/10.1088/1402-4896/ab4923.
- $[17] \ \ M. \ \ W. \ \ Thompson \ Phil. \ Mag. \ \ \textbf{18}, \ (1968) \ \ 377\text{-}414, \ https://doi.org/10.1080/14786436808227358.$
- [18] H. L. Bay and B. Schweer Berichte der Kernforschungsanlage Jülich 2032, (1985).
- [19] R. Behrisch and W. Eckstein "Sputtering by Particle Bombardment", Springer-Verlag p 142.
- [20] A. Mutzke et al. IPP-Report 2019-02, (2019), https://doi.org/10.17617/2.3026474.
- [21] S. Dickheuer et al. Phys. Plasmas 26, (2019) 073513, https://doi.org/10.1063/1.5088931.
- [22] I. Beigman et al. Plasma Phys. Control. Fusion 49, (2007), https://doi.org/10.1088/0741-3335/49/11/006.
- [23] M. S. Benilov, Plasma Sources Sci. Technol. 18, (2009) 014005, https://doi.org/10.1088/0963-0252/18/1/014005
- [24] S. Dickheuer et al., Atoms, 7(48) (2019), https://doi.org/10.3390/atoms7020048.
- [25] W. S. M. Werner et al. J. Phys Chem Ref. Data 38, (2009) 1013-1092, https://doi.org/10.1063/1.3243762.